Chapter 15: Building geological timescales and assigning chronometric time to rocks

Mark W. Hounslow, Graham P. Weedon and David A.T. Harper

Running header: Building geological timescales

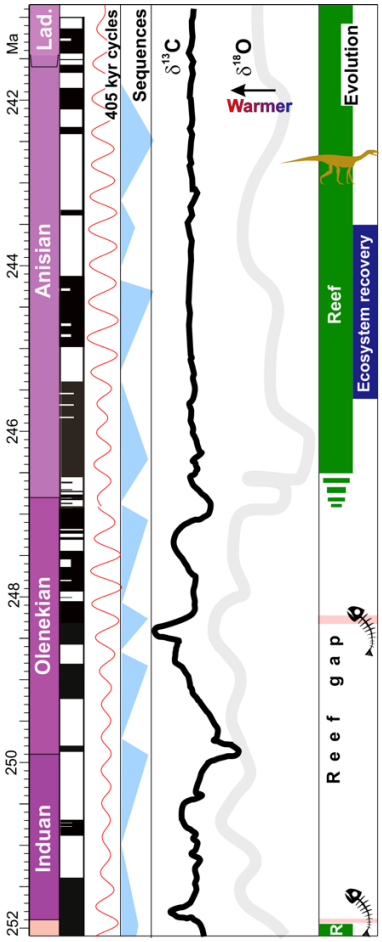

15.1 Introduction

Timescales relate a succession of stratified data points such as fossil first and last occurrences, magnetic polarity boundaries, or isotope excursions, to particular chronometric ages in a linear scale of thousands or millions of years. This process often scales the chronostratigraphical and geochronological divisions of 'rock-time' (as in chapter 13) into million years. It is important to grasp that the rock-time divisions of the International Commission on Stratigraphy's International Chronostratigraphic Chart are not the same as chronometric time, although these become merged in any timescale. Geochronological boundaries (i.e. see Section 13.3) come with no uncertainty in their GSSP-

defined rock-units, but often with significant uncertainty in their correlation and chronometric time.

Timescale construction is typically performed to:

- provide an inter-regional and global assessment of the relative chronometric timing of biotic, chemical and physical changes in Earth history preserved in the geological record;
- calibrate deep-time events (e.g. biozones, stages, and polarity boundaries) to determine their numerical ages and durations (and corresponding uncertainties in time).

Without chronometric time we have no rates. Despite the fact that individual stratigraphical records are inherently incomplete (Section 12.2), geological timescales demonstrate that geological processes span tens to millions and even hundreds of millions of years. Modern timescales integrate information from biostratigraphy, magnetostratigraphy, radioisotope geochronology, chemostratigraphy, climatostratigraphy, sequence stratigraphy and astrochronology (see chapter title page image). Since timescales can be constructed from stratigraphical data from numerous places, they need to be linked together by various means of correlation (Section 17.2). Two widely used examples of timescales are the 'Geologic Time Scale' (Gradstein et al. 2020), and the geomagnetic polarity timescale (Malinverno et al. 2020), with very different datasets and construction methods.

From the early days of geological study, timescales have been produced via various proxy estimators. These included: the rate of sediment accretion on the Nile Delta (Herodotus: 484-409 BCE); rate of the accumulation of salt in the oceans (Edmond Halley: 1656-1742; John Joly: 1857-1933); the thickness of the sedimentary record (John Phillips: 1800-1874); and the cooling of the Earth (William Thomson, Lord Kelvin: 1824-1907). These crude 'rate-based' estimates, are based on uniformitarian principles, and provided early indications of the speed of geological processes. Early in the 20th Century Arthur Holmes, pioneered the use of uranium-series decay curves applied to Precambrian rocks and later to many other parts of the stratigraphical column. Holmes developed the first modern geological timescale, estimating the age of the Earth to be 4,500 Ma ± 100 Myr (Holmes 1956) - close to current estimates. Radio-isotopic dates (yielding chronometric time, Section 13.1) now form one of the key components of timescales.

Timescale or age model? Timescale construction associates many events recorded in rocks, in multiple sections, whilst age-modelling is one (key) method of out of many in timescale construction. Age models relate chronometric time to stratigraphical position from depth or height or a composite-scale position (cf. Sections 4.2.9, 5.5.3). [47 words]

15.2 Time and duration in stratigraphy

Chronostratigraphy (Chapter 13) is codified by the chronostratigraphical charts produced by the International Commission on Stratigraphy (ICS) (https://stratigraphy.org/chart). The 'Geologic Time Scale' books (e.g. the latest; Gradstein et al. 2020 or GTS2020) relate this chronostratigraphy to chronometric time. The presence of fossils, event beds, geochemical and geophysical records and stratigraphical cycles (Chapters 4 to 6 and 8 to 10) permit correlation and targets for dating and/or estimating elapsed time. Subdivisions of geological time (e.g. epochs and periods; Section 13.3) are of uneven duration and often much longer

than any single rock succession. By defining and naming the rock subdivisions (e.g. stages, Sections 13.3 to 13.5), geologists conceptualise the geological rock-time that they represent (e.g. durations) in the same way that, for example, historians might refer to cultural time intervals such as the Mycenaean, Mayan, British Tudors or the Chinese dynasties.

Early, mid- and late. When discussing geochronological units, we use the adjectives early, mid and late, but when dealing with rock we use the terms lower, middle and upper. A fossil is obtained from a level within a rock succession, but the living organism it represents lived during a particular time interval. [52 words, optional]

Early attempts at divisions of strata: Between 1790 and 1840, British, French and German geologists had divided geochronological-time, and familiar terms such as the Silurian, Carboniferous and Cretaceous became common currency. Each geological period (e.g. the Jurassic Period) was defined using the group of sedimentary rock successions called systems considered to date from that time interval (e.g. the Jurassic System). These rock-time units were organised in a vertical column in decreasing order of antiquity, forming the basis for global correlation; with finer subdivisions added later. For example, 19th Century geologists already knew there was a widespread catastrophe or extinction event at the end of the Permian, because rocks of this age could be recognised and correlated across many parts of the globe. Many of the original geological systems as originally defined, were separated from each other by unconformities in their type areas, which aided their local recognition. However, modern epoch/stages and period/system boundaries are defined in stratigraphically complete sections using 'golden spikes' or Global Stratigraphical Sections and Points (GSSPs, Section 13.5).

15.2.1. Time tools

The key modern methods for measuring and interpreting time from rocks and building timescales are summarised in Table 15.1 (chapter numbers indicate sources of further methodological guidance). These are divided into primary means, based on fundamental physical properties that yield chronometric dates or durations, and secondary time-tools, which provide dates (with uncertainty) when calibrated to chronometric time. Two examples: (1) Cody et al. (2008) derived a timescale for southern-ocean diatom first- and last-occurrences, with data derived from 37 cores and sections. They used constrained optimization (CONOP, Sections 4.2.9, 12.3 and 17.2) to generate a composite biostratigraphical scale tied to 52 secondary dates from geomagnetic polarity boundaries (Section 5.3), with ages from Gradstein et al. (2004) and two primary dates from $^{40}Ar/^{39}Ar$ dated tephras (1σ uncertainty of 0.11 - 0.14 Myr). (2) Davydov et al. (2010) generated a timescale of fusulinid-conodont zonations from the Carboniferous of the Donetz Basin, Ukraine. The zonation is connected to a detailed lithostratigraphy, with the durations derived from inferred (glacially driven) 100 and 400 kyr parasequences (Section 8.2), plus 12 U-Pb primary dates (Section 14.1).

Dates from tephra are often the key points for measuring the radio-isotopic age of rock successions (Section 14.2). In marine successions these are of great value for age models, especially if from multiple levels, when combined using Bayesian age models (now routinely used in radiocarbon chronologies). In the absence of dateable tephra, magmatic detrital zircons (for U-Pb dating) and sanidines (for $^{40}Ar/^{39}Ar$ dating) can provide approximate

maximum-depositional ages from the youngest grains in large datasets, given suitable protocols for selection (Spencer et al. 2016). Whilst, unlikely to yield deposition ages as accurate as tephra, these are useful in non-marine, some biota-poor marine settings and in non-marine strata (Section 17.3). In Quaternary strata radiocarbon dating is commonly used. In GTS2020 a wide range of different tools and methods have been used for different time intervals (see figure 1.3 in Gradstein et al. 2020 and Agterberg et al. 2020).

Table 15.1. The key primary[p] and secondary[s] tools (see footnote) for measuring and interpreting time from rocks and sediments. [300 words, page width, ½ page]

Time Tool	Method and calibration method	Key limitations
Archaeological artifacts and events[P]	e.g. coins or historical events of known date.	Limited to coins and historical events in last ~5000-3000 yr
Radio-isotopic dating of primary igneous events (e.g. tephra), Re-Os dating of organic-rich mudrocks, Carbon dating of organic matter [P]	Dependent on radioactive decay rates of mother-daughter products (Chapter 14).	Precision dependent on isotopic system, often limited stratigraphical occurrences.
Astrochronology[P]	Orbital tuning of stratigraphical time series to calculated history of orbital cycles or floating astronomical timescale by recognising regular cycles of set duration (Section 9.4.3)	Dependent on demonstration of astronomical cycles in sediments. Full orbital tuning restricted to last 40 Myr. Tuning to 405 kyr orbital cycles requires high precision radio-isotopic anchors. Mostly floating astrochronologies from Palaeozoic and Mesozoic strata.
U/Pb dating of detrital zircons, $^{40}Ar/^{39}Ar$ dating of detrital sanidine[p]	Dependent on radioactive decay rates of mother-daughter products.	Dependent on 'time of deposition' grains (Spencer et al. 2016). Useful in some tephra-absent strata.
Tephrochronology[S]	Needs dating via primary means.	Limited to dated and recognised tephra events (Huff 2016).
Oceanic oxygen isotopic changes[S]	Need dating via primary means (Chapters 6 and 10).	Only well calibrated for the Quaternary (Section 10.3.2).
Geomagnetic polarity boundaries[S]	Need dating via primary or other secondary means (Chapter 5).	Only well calibrated since the Tithonian (Section 5.3). Not recoverable from some successions.
Global changes in stable carbon isotopic changes[S]	Need dating via primary or other secondary means (Chapter 6).	Only applicable where there are global changes in the carbon cycle, for instance oceanic anoxic events and other palaeoclimatic events such

		as the PETM. Limited events in time, diagenetic changes limit application.
Chronostratigraphical boundaries [S], including GSSPs	Need dating via primary means or other secondary (Chapters 8 and 13).	Dependent on correlation and interpretational accuracy, sometimes ill-defined or large uncertainties

[P]= Primary tools relating to underlying physical laws [S]=Secondary type tools requiring calibration by primary time-tools.

15.3. Initial stages of timescale creation

Timescale creation can use datasets in various formats (dataset column in Fig. 15.1). If the data are derived from a single section or core in depth or height then, given a set of suitable dates or durations, an algorithm can be used to generate an *age model* for this succession - i.e. a continuous age model with depth (Section 15.5).

With more complex multi-location datasets, as is more typical, it is necessary to derive a *composite scale* (in composite scale units: CSU) for the stratified dataset, from the individual cores or sections prior to generating the age-model (Fig. 15.1 and Section 15.4). Hence, for many timescales, the first task is to merge data into a composite-scale, using correlation (i.e. correlations at ticks on schematic columns in Fig. 15.1). This is followed by the development of the age model against the units of the composite scale (Section 15.5).

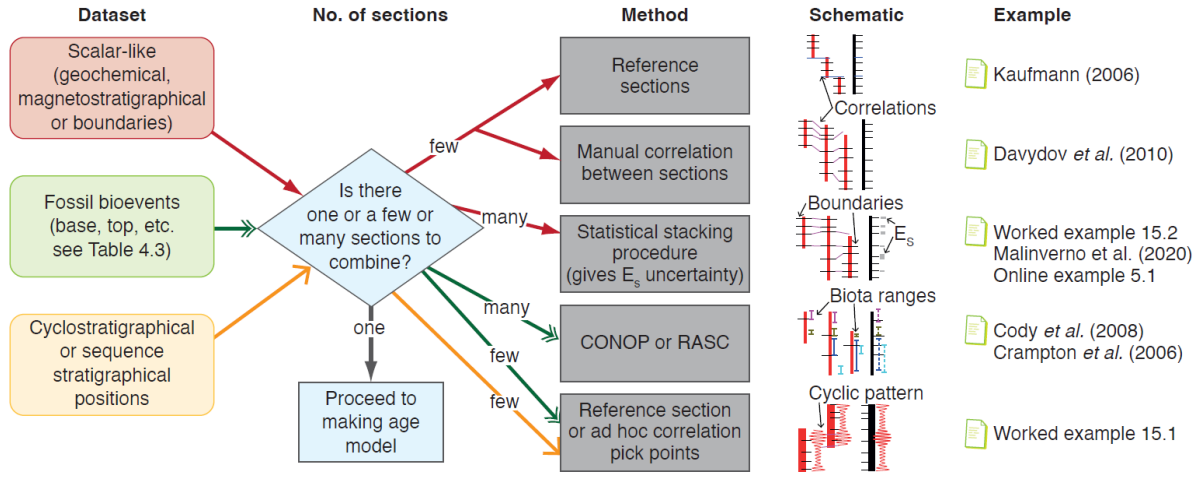

Fig. 15.1. Decision tree for making a stratigraphical composite scale of the data being studied. See Section 17.2 for more on constrained optimisation (CONOP) and ranking and scaling (RASC), and Chapter 4 for palaeontological data. Schematic sketch shows source section in red with black horizontal stratigraphical boundaries, and composite section in black. E_s is the stratigraphic uncertainty of the boundary from statistical stacking procedures. [page width to ensure schematics are readable, 7 cm height = 1/3 page]

15.3.1 Correlation basics

In the process of making composite-scales the correlation of a datum (e.g. biozone, magnetozone boundaries) between rock successions is a fundamental part of the process of relating events. Traditionally most epoch and stage boundaries are correlated by biological markers often using the first appearance of an easily recognisable species within an evolving lineage, that ideally has a short time range and a widespread distribution across facies and latitudes (see Sections 4.2.7, 17.2). Over regional and even local scales, bioevents are

usually more synchronous than lithological contacts (Worked example 1.3, Section 4.2.8). Non-biological means of correlation (such as using marine oxygen isotope data from the Cenozoic), or variations in carbon and strontium isotopes and magnetostratigraphy may provide additional markers to augment or replace biozonal correlation (Sections 5.3, 6.2).

Quantitative bio-correlation can be achieved by comparing the vertical distributions of both biological and nonbiological markers or by using a range of computer-based algorithms (Section 17.2). Important for palaeontological data is the method of graphic correlation that allows comparison of pairs of sections – highlighting previously undetected local stratigraphical gaps (Sections 8.3.3, Figs. 12.9, 12.10, Section 17.2.2; Worked examples 9.1, 12.1). Automated assimilation of hundreds of graphic correlation plots is possible using CONOP software (Section 17.2; Sadler 2020). This compiles data from multiple sites, producing a composite stratigraphy that estimates the likely full stratigraphical ranges of biota.

15.3.2 Synchroneity and uncertainty in correlation and dates

However, over large distances it is hard to demonstrate synchrony of biotic events. Ideally very precise radio- isotopic dates from a boundary at multiple locations are required to demonstrate event synchrony. Alternatively, a biostratigraphical boundary may consistently relate to a magnetic polarity or geochemical boundary. As such stratigraphical correlation, as needed in creation of composite-scales, always comes with some stratigraphical uncertainty (see Section 17.2 also).

In deep time, chronometric ages are commonly used by correlating some or all of the radio-isotopic dates onto the composite scale. This correlation usually comes with some stratigraphic uncertainty, E_s, in the scale of the composite. A radio-isotopic date when located in a section used in the composite has E_s=0. The radio-isotopic date uncertainty used (symbolised here as E_r) should include analytical, tracer and decay constant uncertainties (see Section 14.4.3). Dates used in age-model creation are normally provided as 1σ, rather than the 2σ often quoted on the radio-isotopic dates themselves. Furthermore, the uncertainties that arise from timescales constructed using dates from different isotopic systems (e.g. U-Pb versus $^{40}Ar/^{39}Ar$) should be taken into account (e.g. Worked example 15.1). Uncertainties in astrochronologies are explored in Sections 9.4.3 and 15.5.1.

Stratigraphic uncertainty here symbolised as E_s; expressed in thickness, time or CSU units, with E_s as maximum-minimum range, or 1σ range. The extent to which E_s can be utilised (or even defined) is method-dependent. Numerical compositing methods may generate this uncertainty as part of the process. **[46 words]**

15.4 Construction of composite stratigraphical scales

A range of methods have been used for making composite scales, which are in part dependent upon the kind and amount of data available (method in Fig. 15.1, Table 15.2). Where data are non-biological scalars and few in number, stacking datasets may be suitable, perhaps using an approach based on a standard reference section (Langereis and Hilgen 1991), or stacked depths (Prell et al. 1986), astronomical cycles (Li et al. 2016) or even

parasequences (Davydov et al. 2010). If using a reference section approach (e.g. Section 4.2.9), this would generate a composite with the scale of the reference sections, and if using methods from cyclostratigraphy, a composite with cumulative time from orbital tuning (Worked example 9.1). Other approaches use statistical composites that average the position of events from many sections by making assumptions about smoothing and modelling the distribution of the data, to minimize implied accumulation rate changes across multiple sections (Lisiecki and Lisiecki 2002; Malinvero et al. 2020). Simple examples of statistical composite section construction are given in Worked example 15.2 and online Worked example 5.1 (GIP/DEH/5-tbd).

Table 15.2. Summary of the methods used in creating composite stratigraphical scales.
[267 words, page width = 1/3 page, place in section 5.3.1]

Data type	Example	Description	Method reference	Software
Cycle-scaling				
Astronomical cycle-scaling	Li et al. 2016	Scale generated by 'tuning' mathematically proven regular cycles to an astronomical history		*Ad hoc* correlations and pick points
Parasequence cycle-scaling	Davydov et al. 2010	Scale generated by 'tuning' cycles that are inferred to be regular to a fixed duration.		*Ad hoc* correlations and pick points
Quantitative scalar data				
Reference section stacking	Miller et al. 1991	Stacks quantitative data (e.g. isotope, cycles, magnetic)	Langereis and Hilgen 1991	*Ad hoc* correlations and pick points
Multi section stacking	Prell et al. 1986	Graphic-correlation based stacking	Prell et al. 1986; Lisiecki and Lisiecki 2002	Match, Autocomp, HMM-Stack (UNIX, Matlab). lorraine-lisiecki.com
Multi section statistical stacking	Hounslow and Balabanov 2018	Statistical best position based on simple accumulation rate models	Hounslow, 2016	Spreadsheet and Excel solver
Statistical stacking, using dates as control	Mudelsee et al. 2012	Composite stacking procedure linked to dates, and Monte-Carlo uncertainty	Fohlmeister 2012	Iscam (Matlab script)
Markov chain Monte Carlo algorithm		Minimises the variation of accumulation (or spreading) rate	Malinvero et al. 2020	none
Biotic events, e.g. Base and top events				
CONOP	Serra et al. 2019	Program searches for a global (composite) sequence of events with minimal total amount of range	Sadler et al. 2008; Sadler 2020	PAST 4.05, CONOP9

		extension (set as a penalty) in the individual wells/sections.		
Ranking and Scaling (RASC)	Agterberg et al. 2013	Creates an optimum sequence of events observed in different wells or sections subject to stratigraphical inconsistencies with respect to composite position.	Agterberg et al. 2013	PAST 4.05, RASC-CASC (http://www.nhm2.uio.no/rasc/)

Unlike physical (e.g. geomagnetic) and geochemical data, palaeontological data is often synthesised using compositing and correlation approaches, such as in CONOP and RASC (Fig. 15.1, Table 15.2; Section 17.2). These produce a composite scale (in composite scale units, CSU) related to the rate of evolutionary change implied by the spacing of biozones, which in the case of CONOP can be automatically scaled to chronometric time (e.g. Cody et al. 2008). Making a composite scale using any of these methods is normally at a resolution more detailed than any stage-based chronostratigraphy (Sadler 2020).

15.5 Construction of age-models

An age model relates either a composite scale section, or a section in depth or height to chronometric time. In practice many timescales use the primary chronometric methods in Table 15.1. For this reason we detail astrochronology and radio-isotopic based ages models in the sections below. However, some may also use dates from secondary timescales constructed, such as the geomagnetic polarity timescale (e.g. Cody et al. 2008), or combinations of the tools in Table 15.1. Additional new primary chronometric data produced after a timescales creation may significantly influence the uncertainty in the timescale; consequently users requiring high accuracy and precision are well advised to carefully check the construction of the portion of the timescale they are using.

Time-tools ages Secondary time-tool ages are by their nature of a preliminary character and always have associated chronometric uncertainty, since they are subject to later revisions from primary chronometric dates. This is evident by changes in the geological timescale over the last decades (see figures. 1.5 and 1.6 of Gradstein et al. 2020). **[51 words]**

Construction of GTS2020: Much of the Palaeozoic age model creation in Gradstein et al. (2020) is based on smoothing cubic spline based age modelling. This uses deviations of radio-isotopic data from the spline to estimate age uncertainty. In contrast for much of the Mesozoic and Cenozoic, astrochronology (Section 15.5.1) with varying degrees of quality control, has been tuned to multiple components of the orbital solution, a single orbital cycle, anchored or floating astrochronologies. These have been additionally anchored using radio-isotopic dates and/or the geomagnetic polarity timescale.

15.5.1 Creating age models from astrochronology

Many sedimentary sections are cyclic (e.g. Fig. 15.2). When regularity can be demonstrated mathematically (Chapter 9) and the cyclicity can be linked to climatic variations controlled by specific Milankovitch orbital cycles (in eccentricity, obliquity and/or precession) an astrochronology can be developed. Since the reliability of orbital solutions is age-dependent, how to deal with such data, and the dating uncertainties, are also age dependent.

Fig. 15.2 The Seaford Chalk Formation of Scratchell's Bay, Isle of Wight, UK (Coniacian, Upper Cretaceous). The alternations of white chalk and thin dark flint bands may result from orbital-climatic (Milankovitch) control of silica dissolution and re-precipitation during early diagenesis (Hart 1987). Lack of bundling indicates the cycles are most likely to relate to orbital obliquity, so each chalk-flint couplet may represent ~40 kyr. The abrupt increase in flint band spacing, a third of the way up the section is interpreted as due to increased accumulation rates. [Text width or less no more than 10 cm high = ½ page + 87 word caption. If space tight could be marginal but not ideal.]

Tuning to the orbital solution (Late Paleogene to Quaternary astrochronologies) For strata younger than late Middle Eocene (40 Ma) cyclic records can be tuned directly to an 'orbital solution' i.e. to a calculated orbital history comprising multiple frequencies (Lourens et al. 2004; Pälike et al. 2006; Sections 9.1.1 and 9.4.3). 'Orbital tuning' allows data in depth to be placed into an age model (Fig. 9.18). After tuning, each cycle of the data series is correlated to the time interval of the target orbital cycles. Hence, one measure of the uncertainty of the tuning (E_c) is the period of the shortest target orbital cycle. In the Quaternary to late Paleogene, the ages of bioevents, geomagnetic reversals and deep-sea sediments oxygen- and carbon-isotope variations, are frequently constrained to a specific precession cycle with an uncertainty of as little as ±20 kyr.

Anchored and floating astrochronologies (prior to the Early Paleogene) Orbital solutions, that are consistent with current observations of planetary orbits, diverge for strata older than 40 Ma, partly due to the chaotic dynamics of the inner solar system and uncertainties in the tidal dissipation (Laskar 2020). Westerhold et al. (2012) showed that back to 50 Ma (mid-Eocene) the orbital solution of Laskar et al. (2011) provides a history of variations in short eccentricity cycles (period ~100 kyr) which can be used for tuning.

However, the precise timing and amplitude of variations in precession and obliquity cannot be determined prior to 40 Ma. The periods of these Milankovitch cycles increase over tens of millions of years because tidal friction causes an increase in the Earth-Moon distance – so Palaeozoic obliquity and precession periods were substantially shorter than today (Berger et al. 1992; Laskar 2020).

The 405 kyr cycle Unlike the short eccentricity cycle (~100 kyr) and the very long or 'grand' eccentricity cycle (~2.4 Myr), the long eccentricity cycle (405 kyr) is exceptionally stable through the Phanerozoic (Laskar 2020). Therefore, 405 kyr variations in eccentricity can be calculated back to at least 250 Ma (earliest Triassic) using equations 4.10 and 4.11 of Laskar (2020). **[61 words]**

The duration of 405 kyr eccentricity cycles means that sections representing less than two million years, either exhibit large changes in accumulation rate and/or have too few 405 kyr cycles for regularity to be demonstrated mathematically. Nevertheless, for Mesozoic to mid Paleogene sections spanning several million years, the 405 kyr eccentricity cycle is invaluable as a tuning target. However, in the absence of precisely dated tie points tuning to 405 kyr cycles only allows transference of the data from depth to time as a floating chronology (Worked example 15.1). Considerable progress has been made for the Late Cretaceous timescale; Meyers et al. (2012) and Sageman et al. (2014) combined a floating 405 kyr astrochronology of Upper Cretaceous strata in the Western Interior Basin, USA with U-Pb dates of zircons and $^{40}Ar/^{39}Ar$ dating of sanidines from identical bentonites. This was possible because these strata appear to be stratigraphically complete at the 405ky scale. This has led to tightly constrained dating of the boundaries of the Turonian, Coniacian and Santonian, with 2σ uncertainty of 0.38 - 0.44 Myr, based on synthesising radio-isotopic, astrochronological and stratigraphical uncertainties.

In the absence of integrated radiometric dates, floating chronologies can only provide minimum durations since it is always possible that cycles are missing at minor hiatuses between particular limits (e.g. Tanner and Lucas 2015; Weedon et al. 2019; Fig. 12.3). Hence, floating astrochronologies should be derived from compositing data from multiple stratigraphical sections to improve the chances of detecting gaps – see Worked example 9.1 and Chapter 12.

Aside from the problem of potentially missing cycles, floating chronologies can suffer from:

- incorrect identification of the orbital cycles recorded stratigraphically
- incorrect data processing (Sections 9.3.2, 9.3.4)
- radio-isotopic dates biased by use of reworked detrital zircons or crystals formed in multiple phases in magma chambers

- incorrect correlation (and/or large E_S) of radio-isotopic -dated events when using cyclostratigraphical data from distant sections.

Some Palaeozoic and Mesozoic stages currently have floating astrochronologies that imply stage durations much longer than obtained by radiometric dating (e.g. Fammenian, Hettangian and Aptian; Gradstein et al. 2020). These discrepancies could be related to one or more of these complications.

Worked example 15.1 Floating astrochronology for the Paleocene

This worked example shows how compositing multiple sections was used to derive an astronomical timescale for an epoch. Westerhold et al. (2008) attempted the first astrochronology for the entire Paleocene (~66-56 Ma). Three globally significant events occur within this interval: the Palaeocene-Eocene Thermal Maximum (PETM, see Worked example 6.1), the Early-late Palaeocene Biotic Event (ELPE) (just older than Selandian-Thanetian boundary) and the Cretaceous-Paleogene (K/Pg) boundary. These events are associated with stable oxygen- and carbon-isotope excursions, increased plankton turnover and shallowing of the lysocline (Westerhold et al. 2008). Having an accurate timescale for this interval was therefore important to aid understanding of palaeoenvironmental changes.

The data used for astrochronology included XRF-derived Fe concentrations in cores from ODP sites 1209, 1210 and 1211 from the Shatsky Rise in the North mid Pacific; ODP sites 1262 and 1267 from the Walvis Ridge in the South Atlantic; and lithological data from the Zumaia site on the coast of northern Spain. Average accumulation rates at Shatsky Rise of 1 cm kyr^{-1} were lower than those on Walvis Ridge at 3 to 1 cm kyr^{-1}. The Shatsky Rise cores lacked a magnetostratigraphy so correlation between regions utilized boundaries of a revised calcareous nannofossil zonations (CNP1 to CNP9 biozones of Agnini et al. 2007).

Spectral analysis of the compositional data, including use of wavelet spectrograms (Section 9.3.5), indicated two scales of regular cyclicity in the North Pacific and the South Atlantic data with a frequency ratio of 1:4 – consistent with 405 and 100 kyr cyclicity. The tuning target was the 405 kyr eccentricity cycles from Laskar et al. (2004) given the age is >40 Ma. Maxima in sediment Fe concentration were treated as in-phase with maxima in eccentricity.

Radiometric dating available in 2008 placed the K/Pg between 66.10 and 65.5 Ma (partly due to differences in dates from $^{40}Ar/^{39}Ar$ and U-Pb dating). This meant it was not possible for Westerhold et al. (2008) to associate the K/Pg boundary with a specific 405 kyr cycle. Their data were orbitally tuned, to remove the effects of varying accumulation rates, to yield a floating chronology. The authors proposed three options for relating their composite floating astrochronology from the South Atlantic to the tuning target (two of which are shown in Fig. 15.3).

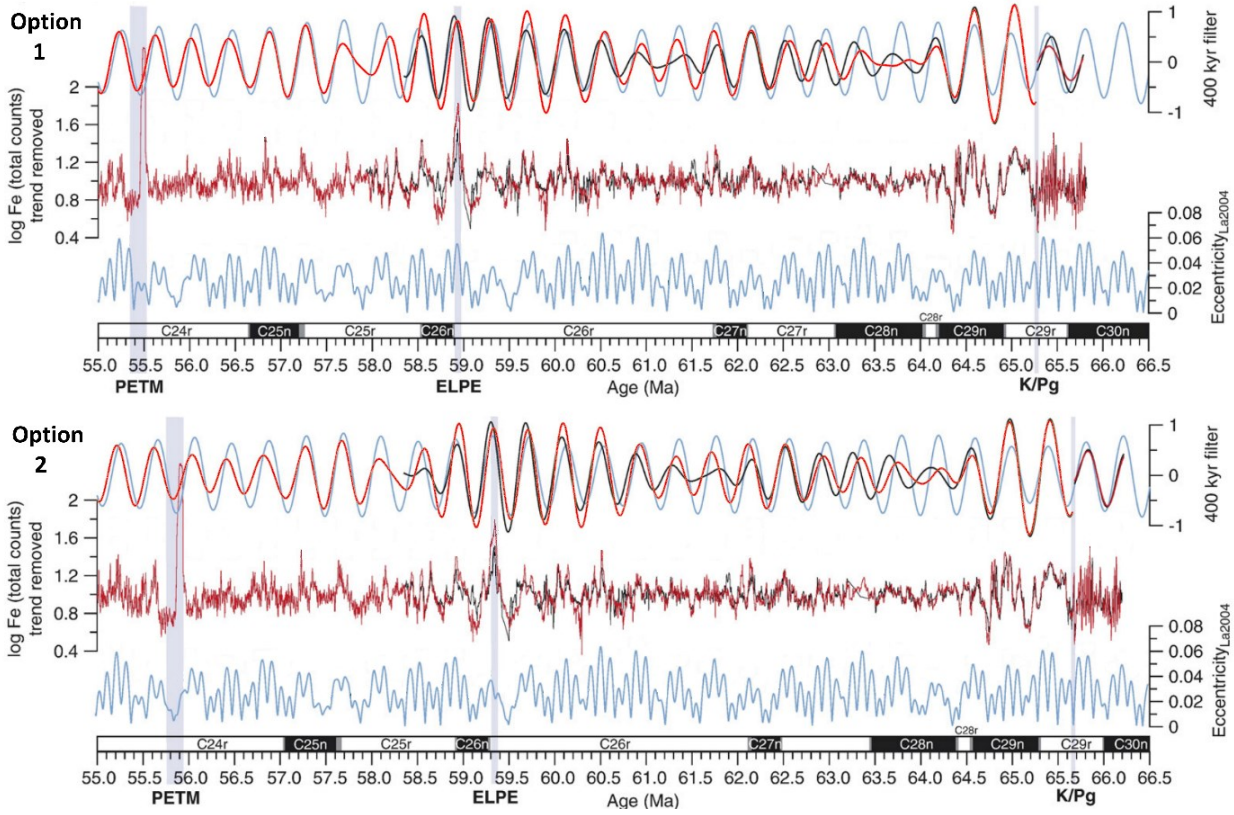

Fig. 15.3. Options 1 and 2 of Westerhold et al. (2008) indicating two possible relationships between data from ODP 1262 (red) and ODP 1267 (black) and the 405 kyr component of the Laskar et al. (2004) orbital solution (blue). The position of three events PETM, ELPE and K/Pg boundary are indicated as vertical grey bars. Modified from Fig. 9 of Westerhold et al. (2008). [Full page width, 11 cm high = ½ page]

Option 1 placed the PETM at 55.53 Ma which implied a date of 65.28 Ma for the K/Pg boundary. Option 2 fixed the PETM at 55.93 Ma, implying 65.68 Ma for the K/Pg boundary (one 405 kyr cycle offset from Option 1). Option 3 was also considered (but was not illustrated), with the PETM at 56.33 Ma, inferring the K/Pg boundary at 66.08 Ma.

Unfortunately, the 405 kyr filter output at ODP 1267 (black in Fig. 15.3) was out of phase relative to both ODP 1262 (in red) and the Laskar et al. (2004) solution (in blue) at 64.2 to 62.7 Ma in Option 1; and Option 2 at 64.6 to 63.0 Ma. Additionally, data from Shatsky Rise ODP 1209, just above the K/Pg, is in the so-called 'strange interval' which is expanded relative to the Walvis Ridge data at ODP 1262 and 1267. Westerhold et al. (2008) inferred the 'strange interval' represented one 405 kyr, so altogether they identified twenty-four 405 kyr cycles between the PETM and the K/Pg boundary.

The revision of the Westerhold et al. (2008) astrochronology by Dinarès-Turell et al. (2014), implied the presence of three extra short eccentricity cycles in the lowermost Paleocene. Their revised dating agrees (within stratigraphical correlation uncertainty) with the most recent radiometric date for the K/Pg boundary of 66.021 ± 0.024/0.039/0.081 Ma (Clyde et al. 2016).

15.4.2. Creating age-models from radio-isotopic dates

The first challenge is to select the most appropriate method. This depends on access to suitable software, and scripting ability (Fig. 15.4 Table 15.3). Classical age modelling algorithms use: splines (Heegaard et al. 2005; Agterberg et al. 2020); polynomials in linear regression (Bennett 1994); Bezier curves (Bennett and Fuller 2002); fuzzy regression (Boreux et al. 1997); LOESS curves (e.g. Hercman and Pawlak 2012) and others (Blaauw 2010). If estimating the uncertainty of the age model is crucial (as it should be), this may restrict choices within classical age modelling (Telford et al. 2004; Blaauw 2010). Some software and methods use Monte-Carlo simulations to determine uncertainty (Scholz and Hoffman 2011; Breitenbach et al. 2012).

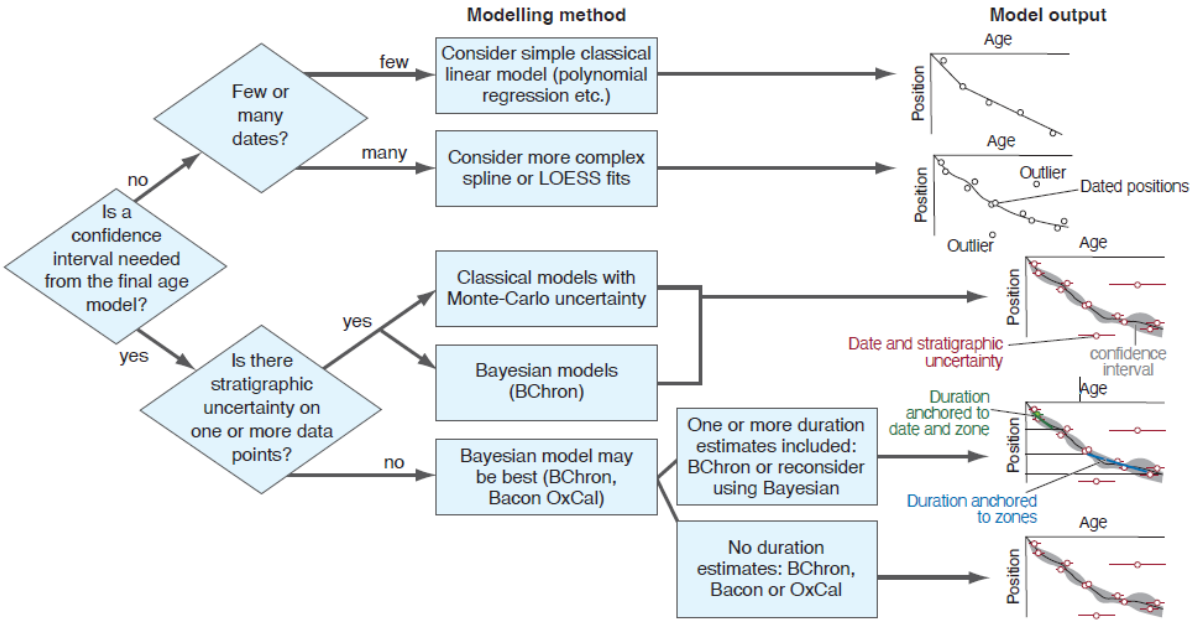

Fig. 15.4. Decision tree on how to make an age model from a composite scale or using a scale in depth or height. Model output shows graphically how the kind of method and data used dictates the uncertainty defined in the output age model. The GTS2020 extensively uses splines (Agterberg et al. 2020). [full page width, 9.5 cm high = 1/3 page]

In recent decades there has been an expansion of more sophisticated age-modelling methods, primarily driven by studies in the Holocene and Quaternary utilising many (some divergent) radiocarbon dates in cores (Parnell et al. 2011) or U-series dates from speleothems (Scholz and Hoffman 2011). Bayesian-based methods (Fig. 15.4, Table 15.3) are being increasingly adopted by the Quaternary community (Lacourse and Gajewski 2020), and will likely be adopted by the deep-time community. Some methods can be readily adapted for deep-time records (De Vleeschouwer and Parnell 2014; Hounslow and Balabanov 2018; Traylor et al. 2019; McKay et al. 2021).

The key considerations in moving from late Quaternary to deep-time age models are:

- The sophistication of Bayesian techniques is partly related to the complexity of using calibrated radiocarbon dates. Using U-Pb or $^{40}Ar/^{39}Ar$ dates removes some complexity

by assuming simple symmetric (Gaussian or uniform distributed) uncertainties. This situation has been adapted for using BChron by implementing more complex probability density functions which can be matched to suit most situations (Traylor et al. 2019). OxCal can also handle tailor-made probability density distributions (Griffiths et al. 2011), but to date OxCal has been little used in deep-time records.

- Re-scaling of the composite scale when using deep-time data will be be needed to match the expectations of the software, which may be designed to work with year dates and use cm-scales and include core-tops at zero years.
- In deep time, timescales are normally constructed by correlating some or all of the radio-isotopic dates (with attendant 1σ uncertainty, E_r) into the composite scale from age-overlapping sections. These sections may not be part of the compositing section-set, so this correlation comes with stratigraphic uncertainty (indicated as E_s in Fig. 15.1), i.e. uncertainty in how the dates relate to the composite scale (Section 15.3.2). Some age-modelling tools, do not allow this kind of uncertainty to be expressed. Those that have some facility for this, express this uncertainty as a sampling interval or *range* (e.g. BChron, 'thickness') in the scale (often with a uniform distribution for this uncertainty). However, in BChron this is currently limited to non-overlapping ranges, since the facility to do this is based on bulk-radiocarbon dates whose sampling intervals may be 10's of cm. Overlapping E_s are not currently catered for in any age modelling methods, so E_s would either need to be restricted to avoid overlap, or the uncertainty and date would have to be combined from the two 'dates' (see section 14A.5.1 in Agterberg et al. 2020).
- Duration intervals from chronometric tools (from floating or anchored cyclostratigraphy, annual layering etc.) are not routinely handled in Bayesian methods. However, for the Devonian, De Vleeschouwer and Parnell (2014) restricted simulations to only include those from the confidence interval of the astronomical duration of the Frasnian and Givetian (R-script for doing this is in online material GiP/DEH/15-1). However, the non-Bayesian methods of Breitenbach et al. (2012) and Scholz and Hoffman (2011) can also include duration estimates. Worked example 15.2 illustrates using astrochronology data with BChron.
- An hiatus in the age model is problematic for most types of age modelling software and methods, and strategies for handling it are either a) segmenting the age model at the hiatus, if it is clearly apparent from the sedimentology and other stratigraphic methods or b) if the hiatus is clearly closely bracketed by date control points, then Bayesian-based age models may express it suitably.

Hybrid age modelling-timescale schemes are also possible, which do not adhere to the composite construction to age model progression in Figs 15.1 and 15.4. For example, the Jurassic-Early Cretaceous timescale in Gradstein et al. (2020) uses a hybrid of anchored and stacked cyclostratigraphical durations (of ammonite zones) for much of the Early Jurassic. For the mid-Jurassic to Early Cretaceous, a sea-floor anomaly-based timescale (spline fit to a few dates, starting in the Albian) is correlated to land-based sections (with ammonite biozones), with additional scaling of ammonite biozone durations based on astrochronology.

Table 15.3. Methods for constructing quantitative age models. [197 words, page width as not those many words in columns? =1/4 page]

Method	E_s/ H/D	Example	Reference	Software
Linear regression with uncertainty in X and Y	Y/N/N		Reed 2010	Excel spreadsheet
Simple age models using linear or polynomial interpolation or splines	N/N/N	Yeloff et al. 2006	Grimm 2000	TiliaIT (www.tiliait.com/) for windows, Tilia for DOS (v.2)
Cubic smooth spline function, including a knot at each dated layer	Y/N/N		Heergard et al. 2005	Parts of R script available.
Age models with uncertainty				
Monte-Carlo simulation of linear segments	Y/Y/Y	Tan et al. 2018	Breitenbach et al. 2012	COPRA (Matlab script), http://tocsy.pik-potsdam.de
LOESS function estimates, with Monte Carlo estimates	Y/N/N	Hercman et al. 2014	Hercman and Pawlak 2012	MOD-Age (windows software)
Monte-Carlo simulation of linear segments	Y/Y/N	Berkelhammer et al. 2012	Scholz and Hoffman 2011	StalAge (R script)
Bootstrap resampling of PDF's, built-in depth uncertainty	Y/N/N		Lougheed and Obrochta 2019	Undatable (Matlab script)
Classical linear, polynomial or cubic splines	N/Y/N	Hubay et al. 2019	Blaauw 2010	Clam (in R)
Bayesian principle-based	N/Y/Y	Staff et al. 2019	Bronk Ramsey 2008	OxCal (P sequence), c14.arch.ox.ac.uk/oxcal.html
Bayesian principle-based	N/Y/N	Sprain et al. 2019	Blaauw and Christen 2011	Bacon (in R)
Bayesian principle-based	Y/N/Y	Trayler et al. 2020	Parnell et al. 2011	Bchron (in R)

E_S= stratigraphical uncertainty can be incorporated into the modelling approach. H- Hiatus can be included in modelling approach, D- duration estimates (e.g. from floating cyclostratigraphy and varves) can be included in the modelling approach. PDF=probability density functions.

Worked example 15.2 Age-model construction: the Devonian

This example of an age-model construction is based on the Devonian timescale created by De Vleeschouwer and Parnell (2014) which used the software package BChron (Table 15.3). They used the reference-section type composite of Kaufmann (2006), but this is modified here as detailed in the online information Excel file, which used Excel solver to make the composite scale **(**see GiP/DEH/15-1**)**. This example starts from this new composite reference

section, which relates the conodont biozone tops (numbered 0 to 69; 70 is the lowest Tournaisian biozone) to the composite scale units (CSU), here 0 to 1000 for base and top of the Devonian (Fig. 15.5). The procedure (Fig. 15.6) follows a slightly different route from De Vleeschouwer and Parnell (2014), since our example uses cyclostratigraphical data both anchored to radio-isotopic dates and unanchored (i.e. as a floating astrochronology).

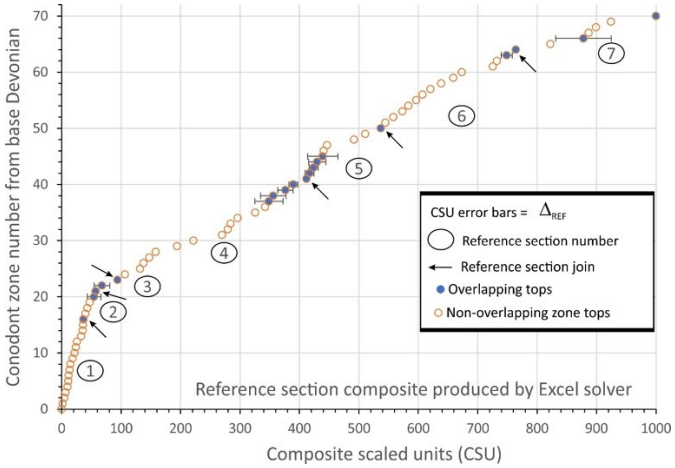

Fig. 15.5. Reference section composite which links the top of conodont zones (Y-axis) to the composite scale units (CSU) on the x-axis. Δ_{REF} = average difference (in CSU) between matching conodont zone tops in overlapping sections (those in blue) and the final CSU value of that zone in the composite. This illustrates for some levels the uncertainty (i.e. Δ_{REF} is an expression of E_s) in making the reference-type composite. The reference section segments 1 to 4 and 6 refer to figs 3 to 7 respectively in Kaufmann (2006). Segment 5 is from Klapper (1997) and segment 7 from Malec (2014). [single column, 6 cm high = 1/8 page]

De Vleeschouwer and Parnell (2014) used radio-isotopic data (labelled D0 to D15) from Appendix-2 in Gradstein et al. (2012), which this example also uses. However, here the latest Famennian part is replaced with data from Myrow et al. (2014) and one date (D10 of Gradstein et al. 2012) is replaced with data from Percival et al. (2018). Radio-isotopic uncertainty (E_r in 1σ) includes decay constant uncertainty, since there is a mix of dating methods. The stratigraphical uncertainty (range in likely correlation, E_S) in relating the dates to the conodont zones, are from Appendix-2 in Gradstein et al. (2012), and these are mapped onto CSU using the conodont zone composite positions (Figs. 15.5 and 15.7; see online Excel file GiP/DEH/15-1).

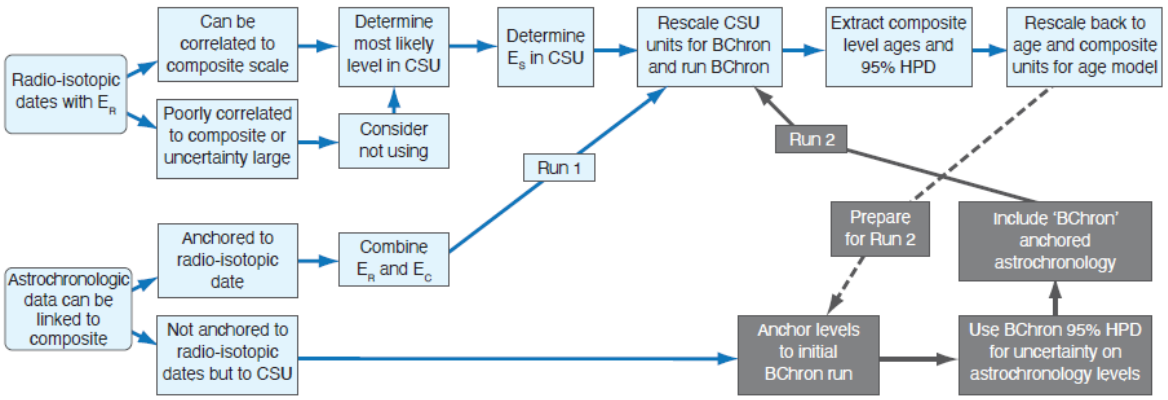

Fig. 15.6. The steps (left to right) used in Worked example 15.2 which includes radio-isotopic dates, and radiometrically anchored and unanchored astrochronology in the age model. The radio-isotopic dates and radiometrically anchored cyclostratigraphy are included in Run-1 (in blue), and any unanchored astrochronology is included in Run-2 (boxes in grey), when the age (with 1σ uncertainty from BChron model) on the zone-boundary anchor point can be determined from Run-1. E_R, E_S and E_C are the 1σ age uncertainty on the radio-isotopic, stratigraphic and astrochronologic values. A floating astrochronology can only be anchored if a reference level in the cyclostratigraphy can be linked to the composite scale; so placing the CSU reference level into the Run-1 output, and so included in the Run-2 of BChron. [page width, 6 cm high = ¼ page]

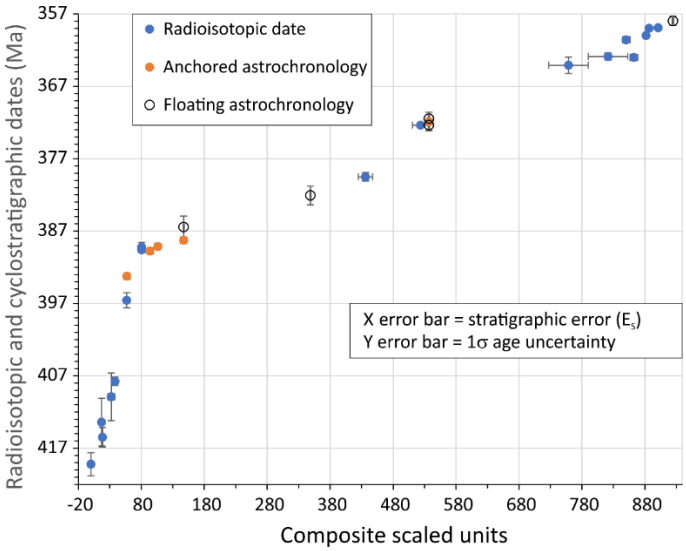

Fig. 15.7. The age control points and uncertainties in mapping the composite scale units (CSU) to age. The floating astrochronology points are attached to the date scale in Run-2 of BChron, others are attached in Run-1. [Single column, 6.5 cm high = 1/8 page]

Some minor modifications to the data were made to make the age model in BChron:

- Duplicate dates at the same position were 'fixed' by adding an offset of 1 CSU (Figs. 15.7, 15.8). The BChron 'jitterPositions' flag failed to work for this dataset, but normally corrects this problem.
- The 'thickness' (Fig. 15.8) variable (scaled E_S) gave overlapping CSU, which causes BChron to fail to run, so for some of the data E_S were reduced to non-overlapping CSU ranges (Fig. 15.8), which slightly decreases the confidence band (highest posterior density (HPD)) around these points.
- The uncertainty (Figs. 15.7, 15.8) of the radio-isotopically-anchored duration from astrochronology is E_R+E_C. For unanchored astrochronology the age uncertainty is E_C plus the 1σ value from Run-1 of BChron at the anchor point in CSU.
- The two Famennian astrochronology durations (Pas et al. 2018; Ma et al. 2020) were anchored to the top of the Famennian (Fig. 15.6), so one top-Famennian date was removed to avoid duplicating data at the top-Famennian.

Predicted ages of the conodont zone boundaries are derived from the Run-2 (Fig. 15.9). In a chronostratigraphical sense the zone boundaries are not without uncertainty when placed in the composite, as is evident by the Δ_{REF} values derived from overlapping portions of the reference sections (Fig. 15.5). Consequently, Δ_{REF} was estimated for all the zone boundaries

by fitting a linear regression trend to the Δ_{REF} values (gets larger for younger intervals, see Gip/DEH/15-1). This was used in the final 95% confidence interval predictions (HPD bands) shown in Fig. 15.9, extracted from the BChron Run-2 data. All these steps are shown in the online Excel file (GiP/DEH/15-1).

Based on a reference scale-type composite this example illustrates how we merge radio-isotopic and cyclostratigraphical duration estimates to generate an age model for the composite scale with realistic confidence intervals, which accounts for all uncertainties.

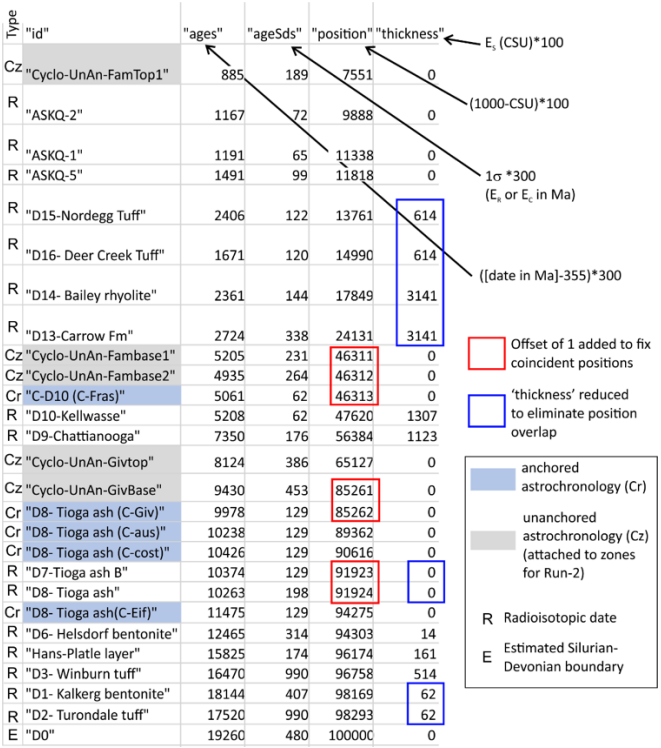

Type	"id"	"ages"	"ageSds"	"position"	"thickness"
Cz	"Cyclo-UnAn-FamTop1"	885	189	7551	0
R	"ASKQ-2"	1167	72	9888	0
R	"ASKQ-1"	1191	65	11338	0
R	"ASKQ-5"	1491	99	11818	0
R	"D15-Nordegg Tuff"	2406	122	13761	614
R	"D16- Deer Creek Tuff"	1671	120	14990	614
R	"D14- Bailey rhyolite"	2361	144	17849	3141
R	"D13-Carrow Fm"	2724	338	24131	3141
Cz	"Cyclo-UnAn-Fambase1"	5205	231	46311	0
Cz	"Cyclo-UnAn-Fambase2"	4935	264	46312	0
Cr	"C-D10 (C-Fras)"	5061	62	46313	0
R	"D10-Kellwasse"	5208	62	47620	1307
R	"D9-Chattianooga"	7350	176	56384	1123
Cz	"Cyclo-UnAn-Givtop"	8124	386	65127	0
Cz	"Cyclo-UnAn-GivBase"	9430	453	85261	0
Cr	"D8- Tioga ash (C-Giv)"	9978	129	85262	0
Cr	"D8- Tioga ash (C-aus)"	10238	129	89362	0
Cr	"D8- Tioga ash (C-cost)"	10426	129	90616	0
R	"D7-Tioga ash B"	10374	129	91923	0
R	"D8- Tioga ash"	10263	198	91924	0
Cr	"D8- Tioga ash(C-Eif)"	11475	129	94275	0
R	"D6- Helsdorf bentonite"	12465	314	94303	14
R	"Hans-Platle layer"	15825	174	96174	161
R	"D3- Winburn tuff"	16470	990	96758	514
R	"D1- Kalkerg bentonite"	18144	407	98169	62
R	"D2- Turondale tuff"	17520	990	98293	62
E	"D0"	19260	480	100000	0

Fig. 15.8. The scaled age and position data for BChron Run-2, formatted as in the input file for BChron (excluding Type column). The last column (not shown) for the BChron file is "normal" for all (indicating the calibration curve type). Those uncoloured in the "id" column are radio-isotopic dates. Annotations show the scaling and fixes to run this age model in BChron. The Run-1 data file for BChron simply excludes those in grey (which are used in Run-2). [Single column width, 9 cm high = 1/6 page]

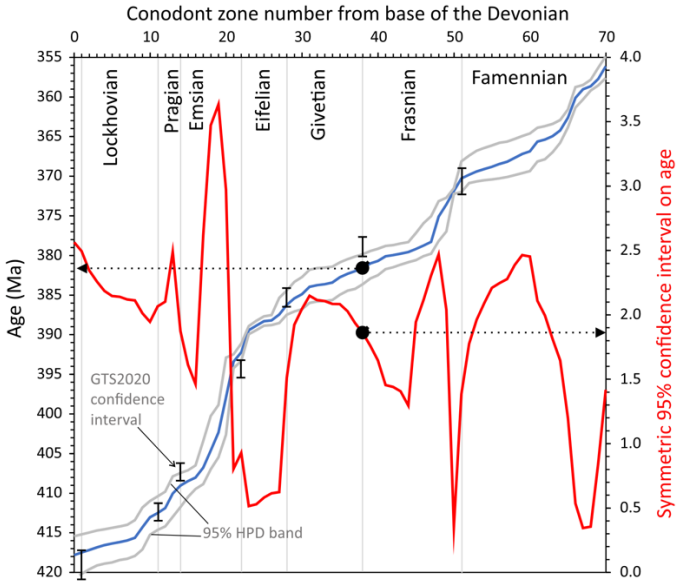

Fig. 15.9. Final age model and 95% confidence intervals for the ages of the 69 conodont zones for the Devonian. From this the most likely ages can be derived. For example, the age of the base Frasnian (zone number 38, MN Zone 1; Klapper 1997) is read off the Y-axis (projection from blue line) at 381.6 Ma and the uncertainty from the red curve is 1.9 Myr (right y-axis). Grey lines are 2.5% and 97.5% HPD, blue line is median (50%) HPD (most likely age) and red-line is ½ the difference between the 2.5% and 97.5% HPD (i.e. a symmetric 95% confidence interval, right hand y-axis). This age model included an estimate of stratigraphical uncertainty (i.e. $E_s \cong \Delta_{REF}$) on the position of all the zone tops, based on the composite-section overlaps (x-axis error bars in Fig. 15.5). For comparison and to show how the approach to constructing a timescale makes a difference, the error bars on the stage bases are the age and 95% uncertainty of the stage ages from Gradstein et al. (2020) using a spline and a slightly different set of control points. [single column, 6.5 cm high = 1/8 page]

15.5 Conclusions

The geological timescale and International Chronostratigraphic Chart are based on principles established many hundreds of years ago, underpinning the definition of the geological systems in the 18th and 19th centuries and later refined. These landmark achievements provide a common language to discuss Earth history, however without the attachment of chronometric dates, their contribution to understanding the timing and rates of biological and geological processes would be limited.

The construction of geological timescales is a multidisciplinary project, requiring the integration of many strands of geological data; the majority of this data is factual, based on the observed distributions and ranges of biological and non-biological phenomena. The methodologies of constructing a composite stratigraphic scale use a variety of data that may be (i) cycle-scaled, (ii) developed from linear-scaled successions of strata or (iii) are focussed on the arrangement and management of fossil range data. Interregional correlation of datasets is a key part of this process. These data may be transferred into age-models for

rock successions, allowing their transformation into numerical ages using Bayesian and other numerical techniques.

Timescales can now be developed across a range of marine and terrestrial facies and confidence intervals may be calculated for the key methods currently in use. Nevertheless, the construction of timescales would benefit from more consistency in approach. Some geological time intervals have well-developed and sophisticated approaches, which however are only applicable to specific regions of the world. The advent of more integrative and sophisticated stratigraphical studies, taking full and well-characterised account of all uncertainty, will aid a strengthened focus on the enhancement of chronostratigraphies with timescales.

Acknowledgements: David Rey, Kirsty Edgar and Phil Gibbard provided constructive reviews.

Further Reading

Agterberg, F.P., Da Silva A-C. and Gradstein, F.M. 2020. 14A.Geomathematical and Statistical Procedures. *In*: Gradstein, F.M., Ogg, J.G., Schmitz, M.D. and Ogg, G.M. eds., 2020. *Geologic time scale 2020*. Elsevier. pp. 401-424. doi.org/10.1127/nos/2020/0634. [Key reading to understand uncertainty and method used in GTS2020]

Blaauw, M., 2010. Methods and code for 'classical'age-modelling of radiocarbon sequences. *Quaternary Geochronology*, **5**, 512-518. doi.org/10.1016/j.quageo.2010.01.002 [good review of age modelling]

Cody, R.D., Levy, R.H., Harwood, D.M. and Sadler, P.M., 2008. Thinking outside the zone: high-resolution quantitative diatom biochronology for the Antarctic Neogene. *Palaeogeography, Palaeoclimatology, Palaeoecology*, **260**, 92-121. doi.org/10.1016/j.palaeo.2007.08.020. [timescale using primary and secondary time-tools and CONOP]

De Vleeschouwer, D. and Parnell, A.C., 2014. Reducing time-scale uncertainty for the Devonian by integrating astrochronology and Bayesian statistics. *Geology*, **42**, 491-494. doi.org/10.1130/G35618.1 [Key reading for worked example]

Dinarès-Turell, J., Westerhold, T., Pujalte, V., Röhl, U. and Kroon, D., 2014. Astronomical calibration of the Danian stage (Early Paleocene) revisited: settling chronologies of sedimentary records across the Atlantic and Pacific Oceans. *Earth and Planetary Science Letters*, **405**, 119-131, doi.org/10.1016/j.epsl.2014.08.027. [good example of cyclostratigraphy use]

Hounslow, M. W. 2016. Geomagnetic reversal rates following Palaeozoic superchrons have a fast restart mechanism. *Nature Communications*, **7**, 12507, doi.org/10.1038/ncomms12507 [a simple statistical compositing method]

Klapper, G. 1997. Graphic correlation of Frasnian (Upper Devonian) sequences in Montagne Noire, France, and western Canada. *Special Papers-Geological Society of America*, **321**, 113-130. doi.org/10.1130/0-8137-2321-3.113. [source for worked example, and example of graphic correlation]

Lacourse, T. and Gajewski, K., 2020. Current practices in building and reporting age-depth models. *Quaternary Research*, **96**, 28-38. doi.org/10.1017/qua.2020.47 [useful review of age models construction]

Langereis, C.G. and Hilgen, F.J., 1991. The Rossello composite: a Mediterranean and global reference section for the Early to early Late Pliocene. *Earth and Planetary Science Letters*, **104**, 211-225. doi.org/10.1016/0012-821X(91)90205-V [example of reference section construction]

Lisiecki, L.E. and Lisiecki, P.A., 2002. Application of dynamic programming to the correlation of paleoclimate records. *Paleoceanography*, **17**, doi.org/10.1029/2001PA000733. [method for composite section construction]

Ma, K. and Li, M. 2020. Astronomical time scale of the Turonian constrained by multiple paleoclimate proxies. *Geoscience Frontiers,* **11**, 1345–1352. doi.org/10.1016/j.gsf.2020.01.013 [assessment of uncertainties in astrochronologies]

Meyers, S.R., Siewert, S.E., Singer, B.S., Sageman, B.B., Condon, D.J., Obradovich, J.D., Jicha, B.R. and Sawyer, D.A., 2012. Intercalibration of radioisotopic and astrochronologic time scale for the Cenomanian-Turonian boundary interval, Western Interior Basin, USA. *Geology*, **40**, 7-10, doi.org/10.1130/G32261.1 [good example of astrochronology use]

McKay, N.P., Emile-Geay, J. and Khider, D., 2021. geoChronR–an R package to model, analyze, and visualize age-uncertain data. Geochronology, **3**, 149-169. doi.org/10.5194/gchron-3-149-2021 [access to a variety of modelling tools in Table 15.4]

Parnell, A.C., Buck, C.E. and Doan, T.K., 2011. A review of statistical chronology models for high-resolution, proxy-based Holocene palaeoenvironmental reconstruction. *Quaternary Science Reviews*, **30**, 2948-2960. doi.org/10.1016/j.quascirev.2011.07.024 [good review of Bayesian age models]

Prell, W.L., Imbrie, J., Martinson, D.G., Morley, J.J., Pisias, N.G., Shackleton, N.J. and Streeter, H.F., 1986. Graphic correlation of oxygen isotope stratigraphy application to the late Quaternary. *Paleoceanography*, **1**, 137-162. doi.org/10.1029/PA001i002p00137. [use of correlation and composite construction]

Sadler, P., 2020. 14B. Global composite sections and constrained optimization. *In:* Gradstein, F.M., Ogg, J.G., Schmitz, M.D., and Ogg, G.M. (eds) *Geologic Time Scale 2020*. Elsevier, Amsterdam, 425-439. doi.org/10.1127/nos/2020/0634. [assessment of use of CONOP for in constructing the GTS2020]

Trayler, R.B., Schmitz, M.D., Cuitiño, J.I., Kohn, M.J., Bargo, M.S., Kay, R.F., Strömberg, C.A. and Vizcaíno, S.F., 2020. An improved approach to age-modelling in deep time: Implications for the Santa Cruz Formation, Argentina. *Geological Society of America Bulletin*, **132**, 233-244. doi.org/10.1130/B35203.1. [Adaption of radioisotopic age uncertainties for Bayesian models]

Weedon, G.P., Page, K.N. and Jenkyns, H.C. 2019. Cyclostratigraphy, stratigraphic gaps and the duration of the Hettangian Stage (Jurassic): insights from the Blue Lias Formation of southern Britain. *Geological Magazine*, **156**, 1469-1509, doi.org/10.1017/S0016756818000808 [great integration of stratigraphic datasets to generate a timescale for the Hettangian]

Other references

Agnini, C., Fornaciari, E., Raffi, I., Rio, D., Rohl, U. and Westerhold, T., 2007. High-resolution nannofossil biochronology of middle Paleocene to early Eocene at ODP Site 1262: implications for calcareous nannoplankton evolution. *Marine Micropaleontology*, **64**, 215-248, doi.org/10.1016/j.marmicro.2007.05.003.

Agterberg, F.P., Gradstein, F.M., Cheng, Q. and Liu, G., 2013. The RASC and CASC programs for ranking, scaling and correlation of biostratigraphic events. C*omputers and Geosciences*, **54**, 279-292. doi.org/10.1016/j.cageo.2013.01.002.

Bennett, K.D., 1994. Confidence intervals for age estimates and deposition times in late-Quaternary sediment sequences. *The Holocene*, **4**, 337-348. doi.org/10.1177/095968369400400401

Bennett, K.D., Fuller, J.L., 2002. Determining the age of the mid-Holocene Tsuga canadensis (hemlock) decline, eastern North America. *The Holocene*, **12**, 421-429. doi.org/10.1191/0959683602hl556rp

Berger, A., Loutre, M. F. and Laskar, J. 1992. Stability of the astronomical frequencies over the Earth's history for paleoclimate studies. *Science*, **255**, 560–566. doi.org/10.1126/science.255.5044.560

Berkelhammer, M., Sinha, A., Stott, L., Cheng, H., Pausata, F.S. and Yoshimura, K., 2012. An abrupt shift in the Indian monsoon 4000 years ago. *Geophysical Monograph Series*, **198**, 75-87. doi.org/10.1029/2012GM001207

Blaauw, M. and Christen, J.A., 2011. Flexible paleoclimate age-depth models using an autoregressive gamma process. *Bayesian Analysis*, **6**, 457-474. doi.org/10.1214/ba/1339616472

Boreux, J.J., Pesti, G., Duckstein, L. and Nicolas, J., 1997. Age model estimation in paleoclimatic research: fuzzy regression and radiocarbon uncertainties. *Palaeogeography, Palaeoclimatology, Palaeoecology*, **128**, 29-37. doi.org/10.1016/S0031-0182(96)00014-4

Breitenbach, S.F.M., Rehfeld, K., Goswami, B., Baldini, J.U., Ridley, H.E., Kennett, D.J., Prufer, K.M., Aquino, V.V., Asmerom, Y., Polyak, V.J. and Cheng, H., 2012. Constructing proxy records from age models (COPRA). *Climate of the Past*, **8**, 1765-1779. doi.org/10.5194/cp-8-1765-2012.

Bronk Ramsey, B., 2008. Deposition models for chronological records. *Quaternary Science Reviews*, **27**, 42-60. doi.org/10.1016/j.quascirev.2007.01.019

Clyde, W.C., Ramezani, J., Johnson, K.R., Bowring, S.A. and Jones, M.M., 2016. Direct high-precision U-Pb geochronology of the end-Cretaceous extinction and calibration of Paleocene astronomical timescales. *Earth and Planetary Science Letters*, **452**, 272-280, doi.org/10.1016/j.epsl.2016.07.041

Crampton, J.S., Schiøler, P. and Roncaglia, L., 2006. Detection of Late Cretaceous eustatic signatures using quantitative biostratigraphy. Geological Society of America Bulletin, **118**, 975-990. doi.org/10.1130/B25826.1

Davydov, V.I., Crowley, J.L., Schmitz, M.D. and Poletaev, V.I., 2010. High-precision U-Pb zircon age calibration of the global Carboniferous time scale and Milankovitch band cyclicity in the Donets basin, eastern Ukraine. *Geochemistry, Geophysics, Geosystems*, **11**, doi.org/10.1029/2009GC002736.

Fohlmeister, J., 2012. A statistical approach to construct composite climate records of dated archives. *Quaternary Geochronology*, **14**, 48-56. doi.org/10.1016/j.quageo.2012.06.007

Gradstein, F.M., Ogg, J.G., Schmitz, M.D. and Ogg, G.M. eds., 2012. *The geologic time scale 2012*. Elsevier. /doi.org/10.1127/0078-0421/2012/0020

Gradstein, F.M., Ogg, J.G., Schmitz, M.D. and Ogg, G.M. eds., 2020. *Geologic time scale 2020*. Elsevier. doi.org/10.1127/nos/2020/0634

Griffiths, S., Bayliss, A., Ford, B.M., Hounslow, M.W., Karloukovski, V., Bronk Ramsey, C., Cook, G. Marshall, P. 2011. Section 19: scientific dating I chronology. In: Ford, B.M and Teague, S. *archaeological excavations between 2002 and 2007 on the sites of Northgate House, Staple Gardens and the former Winchester Library, Jewry St, Oxford Archaeology Monograph 12*, Information Press: Oxford. pp. 225-236.

Grimm, E.C. 2000. TGView and Tilia for windows, 20, *INQUA Sub-Commission on Data-Handling Methods Newsletter* (2000), p. 5

Hart, M.B., 1987. Orbitally induced cycles in the Chalk facies of the United Kingdom. *Cretaceous Research*, **8**, 335-348. doi.org/10.1016/0195-6671(87)90003-6

Heegaard, E., Birks, H.J.B., Telford, R.J., 2005. Relationships between calibrated ages and depth in stratigraphical sequences: an estimation procedure by mixed effect regression. *The Holocene*, **15**, 1-7. doi.org/10.1191/0959683605hl836rr

Hercman, H. and Pawlak, J., 2012. MOD-AGE: An age-depth model construction algorithm. *Quaternary Geochronology*, **12**, 1-10. doi.org/10.1016/j.quageo.2012.05.003

Hercman, H., Gąsiorowski, M. and Pawlak, J., 2014. Testing the MOD-AGE chronologies of lake sediment sequences dated by the 210Pb method. *Quaternary Geochronology*, **22**, 155-162. doi.org/10.1016/j.quageo.2014.01.001

Holmes, A., 1956. How old is the Earth? *Transactions of the Edinburgh Geological Society*, **16**, 313-333. doi.org/10.1144/transed.16.3.313

Hounslow, M.W. and Balabanov, Y.P., 2018. A geomagnetic polarity timescale for the Permian, calibrated to stage boundaries. In: Lucas, S.G and Shen, S.Z. (eds). *The Permian Timescale*, Geological Society, London, Special Publications, **450**, pp. 61-103. doi.org/10.1144/SP450.8

Hubay, K., Molnár, M., Orbán, I., Braun, M., Bíró, T. and Magyari, E., 2018. Age–depth relationship and accumulation rates in four sediment sequences from the Retezat Mts, South Carpathians (Romania). *Quaternary International*, **477**, 7-18. doi.org/10.1016/j.quaint.2016.09.019

Huff, W. 2006. K-bentonites: A review. *American Mineralogist*, **101**, 43-70. doi.org/10.2138/am-2016-5339

Kaufmann, B., 2006. Calibrating the Devonian Time Scale: a synthesis of U–Pb ID–TIMS ages and conodont stratigraphy. *Earth-Science Reviews*, **76**, 175-190. doi.org/10.1016/j.earscirev.2006.01.001

Laskar, J., Fienga, A., Gastineau, M. and Manche, H., 2011. La2010: a new orbital solution for the long-term motion of the earth. *Astronomy and Astrophysics*, **532**, A89, 1-15, doi.org/10.1051/0004-6361/201116836

Laskar, J., Robutel, P., Joutel, F., Gastineau, M., Correia, A.C.M. and Levrard, B., 2004. A long-term numerical solution for the insolation quantities of the Earth. *Astronomy and Astrophysics*, **428**, 261-285, doi.org/10.1051/0004-6361:20041335

Laskar, J. 2020 Astrochronology. In: Gradstein, F.M., Ogg, J.G., Schmitz, M.D. and Ogg, G.M. eds., *Geologic time scale 2020*. Elsevier, pp139-158. doi.org/10.1016/B978-0-12-824360-2.00004-8

Li, M., Ogg, J., Zhang, Y., Huang, C., Hinnov, L., Chen, Z.Q. and Zou, Z., 2016. Astronomical tuning of the end-Permian extinction and the Early Triassic Epoch of South China and Germany. *Earth and Planetary Science Letters*, **441**, 10-25. doi.org/10.1016/j.epsl.2016.02.017

Lyell, C. 1852. A manual of elementary geology, or, the ancient changes of the Earth and its inhabitants as illustrated by geological monuments. https://www.gutenberg.org/files/34350/34350-h/34350-h.htm

Lougheed, B.C. and Obrochta, S.P., 2019. A rapid, deterministic age-depth modelling routine for geological sequences with inherent depth uncertainty. *Paleoceanography and Paleoclimatology*, **34**, 122-133. doi.org/10.1029/2018PA003457

Lourens, L.J., Hilgen, F.J., Laskar, J., Shackleton, N.J. and Wilson, D., 2004. The Neogene Period. In: Gradstein, F., Ogg, J. and Smith, A. (eds), *A Geological Timescale 2004* Cambridge University Press, Cambridge, 409-440. doi.org/10.1017/CBO9780511536045.022

Ma, K., Hinnov, L.A., Zhang, X. and Gong, Y., 2020. Astronomical time calibration of the Upper Devonian Lali section, South China. *Global and Planetary Change*, **193**, doi.org/10.1016/j.gloplacha.2020.103267

Malec, J., 2014. The Devonian/Carboniferous boundary in the Holy Cross Mountains. *Geological Quarterly*, **58**, 217-234. doi.org/10.7306/gq.1142

Malinverno, A., Quigley, K.W., Staro, A. and Dyment, J., 2020. A Late Cretaceous-Eocene geomagnetic polarity timescale (MQSD20) that steadies spreading rates on multiple mid-ocean ridge flanks. *Journal of Geophysical Research: Solid Earth*, **125**, doi.org/10.1029/2020JB020034

Miller, K.G., Feigenson, M.D., Wright, J.D. and Clement, B.M., 1991. Miocene isotope reference section, Deep Sea Drilling Project Site 608: an evaluation of isotope and biostratigraphic resolution. *Paleoceanography*, **6**, 33-52. doi.org/10.1029/90PA01941

Mudelsee, M., Fohlmeister, J. and Scholz, D., 2012. Effects of dating errors on nonparametric trend analyses of speleothem time series. *Climate of the Past*, **8**, 1637-1648. doi.org/10.5194/cp-8-1637-2012

Myrow, P.M., Ramezani, J., Hanson, A.E., Bowring, S.A., Racki, G. and Rakociński, M., 2014. High-precision U–Pb age and duration of the latest Devonian (Famennian) Hangenberg event, and its implications. *Terra Nova*, **26**, 222-229. doi.org/10.1111/ter.12090

Pälike, H. Norris, R.D., Herrle, J.O., Wilson, P.A., Coxall, H.K., Lear, C.H., Shackleton, N.J., Tripati, A.K. and Wade, B.S., 2006. The heartbeat of the Oligocene climate system. *Science*, **314**, 1894-1898, doi.org/10.1126/science.1133822

Pas, D., Hinnov, L., Day, J.E.J., Kodama, K., Sinnesael, M. and Liu, W., 2018. Cyclostratigraphic calibration of the Famennian stage (Late Devonian, Illinois Basin, USA). *Earth and Planetary Science Letters*, **488**, 102-114. doi.org/10.1016/j.epsl.2018.02.010

Percival, L.M., Davies, J.H., Schaltegger, U., De Vleeschouwer, D., Da Silva, A.C. and Föllmi, K.B., 2018. Precisely dating the Frasnian–Famennian boundary: implications for the cause of the Late Devonian mass extinction. *Scientific Reports*, **8**, 1-10. doi.org/10.1038/s41598-018-27847-7

Reed, B.C., 2010. A spreadsheet for linear least-squares fitting with errors in both coordinates. *Physics Education*, **45**, 93-96. doi.org/10.1088/0031-9120/45/1/011

Remane, J., Bassett, M.G., Cowie, J.W., Gohrbandt, K.H. Lane, H.R., Michelsen, O and Naiwen, W. 1996. Revised guidelines for the establishment of global chronostratigraphic standards by the International Commission on Stratigraphy (ICS). *Episodes*, **19**, 77-81. doi.org/10.18814/epiiugs/1996/v19i3/007

Sadler P.M., Kemple W.G., Kooser M.A. 2008. CONOP9 Programs for solving the stratigraphic correlation and seriation problems as constrained optimization. In: Harries P.J. (eds) *High-Resolution Approaches in Stratigraphic Paleontology*. Topics in Geobiology, vol. **21**. Springer, Dordrecht. doi.org/10.1007/978-1-4020-9053-0_13

Sageman, B.B., Singer, B.S., Meyers, S.R., Siewert, S.E., Walaszczyk, I., Condon, D.J., Jicha, B.R., Obradovich, J.D. and Sawyer, D.A., 2014. Integrating 40Ar/39Ar, U-Pb, and astronomical clocks in the Cretaceous Niobrara Formation, Western Interior Basin, USA. *Geological Society of America Bulletin*, **126**, 956-973, doi.org/10.1130/B300929

Scholz, D. and Hoffmann, D.L., 2011. StalAge–An algorithm designed for construction of speleothem age models. *Quaternary Geochronology*, **6**, 369-382. doi.org/10.1016/j.quageo.2011.02.002

Serra, F., Feltes, N.A., Albanesi, G.L. and Goldman, D., 2019. High-resolution conodont biostratigraphy from the Darriwilian Stage (Middle Ordovician) of the Argentine Precordillera and biodiversity analyses: a CONOP 9 approach. *Lethaia*, **52**, 188-203. doi.org/10.1111/let.12306

Speijer, R.P., Pälike, H., Hollis, C.J., Hooker, J.J. and Ogg, J.G., 2020. The Paleogene Period. *In:* Gradstein, F.M., Ogg, J.G., Schmitz, M.D., and Ogg, G.M. (eds) *Geologic Time Scale 2020*. Elsevier, Amsterdam, 1087-1140, doi.org/10.1016/B978-0-12-824360-2.00028-0

Spencer, C.J., Kirkland, C.L. and Taylor, R.J., 2016. Strategies towards statistically robust interpretations of in situ U–Pb zircon geochronology. *Geoscience Frontiers*, **7**(4), pp.581-589. doi.org/10.1016/j.gsf.2015.11.006

Sprain, C.J., Renne, P.R., Vanderkluysen, L., Pande, K., Self, S. and Mittal, T., 2019. The eruptive tempo of Deccan volcanism in relation to the Cretaceous-Paleogene boundary. *Science*, **363**, 866-870. doi.org/10.1126/science.aav1446

Staff, R.A., Hardiman, M., Ramsey, C.B., Adolphi, F., Hare, V.J., Koutsodendris, A. and Pross, J., 2019. Reconciling the Greenland ice-core and radiocarbon timescales through the Laschamp geomagnetic excursion. *Earth and Planetary Science Letters*, **520**, 1-9. doi.org/10.1016/j.epsl.2019.05.021

Tan, L., Cai, Y., Cheng, H., Edwards, L.R., Lan, J., Zhang, H., Li, D., Ma, L., Zhao, P. and Gao, Y., 2018. High resolution monsoon precipitation changes on southeastern Tibetan Plateau over

the past 2300 years. *Quaternary Science Reviews*, **195**, 122-132. doi.org/10.1016/j.quascirev.2018.07.021

Tanner, L.H. and Lucas, S.G., 2015. The Triassic-Jurassic strata of the Newark Basin, USA: a complete and accurate astronomically-tuned timescale? *Stratigraphy*, **12**, 47-65. www.micropress.org/microaccess/stratigraphy/issue-316/article-1933.

Telford, R.J., Heegaard, E. and Birks, H.J.B., 2004. All age–depth models are wrong: but how badly? *Quaternary Science Reviews*, **23**, 1-5. doi.org/10.1016/j.quascirev.2003.11.003

Westerhold, T., Röhl, U., Raffi, I., Fornaciari, E., Monechi, S., Reale, V., Bowles, J. and Evans, H.F. 2008. Astronomical calibration of Paleocene time. *Palaeogeography, Palaeoclimatology, Palaeoecology*, **257**, 377-403, doi.org/10.1016/j.paaeo.2007.09.016.7

Westerhold, T., Röhl, U. and Laskar, J., 2012. Time scale controversy: accurate orbital calibration of the early Paleogene. *Geochemistry, Geophysics, Geosystems*, **13**, Q06015, 1-19, doi.org/10.01029/2012GC004096

Yeloff, D., Bennett, K.D., Blaauw, M., Mauquoy, D., Sillasoo, Ü., van der Plicht, J., van Geel, B., 2006. High precision C-14 dating of Holocene peat deposits: a comparison of Bayesian calibration and wiggle-matching approaches. *Quaternary Geochronology*, **1**, 222-235. doi.org/10.1016/j.quageo.2006.08.003

Chapter 15 title page image: Timescale from Li et al. (2018) for the Early to Mid Triassic, showing time, stages, magnetochrons, astrochronology, sequences, carbon and oxygen isotopes and major evolutional events (pink levels = extinction events).

[Angela's length calculation = 15.92 pages, assumes all table full width. 16 pages allocated, this is word count 12/5 with doi's]